Applied Catalysis B: Environmental 254 (2019) 594–600

Contents lists available at ScienceDirect

Applied Catalysis B: Environmental

journal homepage: www.elsevier.com/locate/apcatb

In situ observation of NiS nanoparticles depositing on single TiO_2 mesocrystal for enhanced photocatalytic hydrogen evolution activity

Xiaowei Shi[a,b], Sooyeon Kim[a], Mamoru Fujitsuka[a], Tetsuro Majima[a,*]

[a] The Institute of Scientific and Industrial Research (SANKEN), Osaka University, Mihogaoka 8-1, Ibaraki, Osaka, 567-0047, Japan
[b] State Key Laboratory Breeding Base of Green Chemistry Synthesis Technology, Zhejiang University of Technology, Hangzhou, 310032, PR China

ARTICLE INFO

Keywords:
In situ
Photoluminescence
Photodeposition
Hydrogen evolution
Heterostructure

ABSTRACT

For photocatalysis, clarifications of charge carrier migration route and kinetics on individual particles by photoluminescence (PL) are of great importance because they play significant roles on unveiling the precise information of structure-activity relationships and closely relate to the photocatalytic activities of those semiconductors on targeted functions. Here, photodeposition process of NiS nanoparticles on single TiO_2 mesocrystal (TMC) as co-catalyst is *in situ* monitored by PL images and spectra using a confocal single-particle PL microscopy, which provides straightforward results on understanding the photoexcited electrons transfer in both individual TMC and TMC/NiS nanoparticles. Through the changes in PL intensity and decay lifetime, preferential trapping site for NiS nanoparticles on TMC is identified and efficient electron interfacial migration from TMC to NiS nanoparticles is demonstrated, which lead to an almost 71 folds enhancement on the photocatalytic H_2 evolution under 365-nm photoirradiation compared to pure TMC particles.

1. Introduction

Owing to the generation of more than 85% transportation fuels and chemicals, solid materials, especially nanomaterials, used as heterogeneous catalysts become more and more significant [1]. Tremendous efforts have been devoted to study the chemical reactions on those ensemble powder materials [2,3]. Even though a part of catalytic properties can be explained according to ensemble-averaged phenomena, it is still difficult to unveil the precise properties of an individual particle hidden in whole sample due to the inherent heterogeneity among nanoparticles in size, shape, and structure. Therefore, monitoring the chemical reactions under the reactive conditions on single particle scale to understand the reaction dynamics deeply and establish structure-reactivity relationships come out from scarcity of methods for such an *in situ* analysis with real time resolution [4–8].

As a new class of porous TiO_2 materials, TiO_2 mesocrystal (TMC) superstructure with micrometer size and regular shape composed by TiO_2 nanocrystals has drawn much attentions [9–11]. Due to the exposure of {001} and {101} facets as the basal and lateral planes, respectively, of TiO_2 nanocrystals to form homojunction, as well as the well-ordered architecture, charge separation efficiency and electron transport distance in TMC is greatly enhanced compared with traditional TiO_2 particles [9,12,13]. The single-molecule measurements by the photocatalytic reduction of a nonfluorescent molecule (3,4-dinitrophenyl-BODIPY, DN-BODIPY) to a fluorescent product (4-hydroxyamino-3-nitrophenyl-BODIPY, HN-BODIPY) demonstrated that the photogenerated electrons could transport as far as micrometer distance within TMC and be preferentially trapped at the lateral of TMC [10].

Nevertheless, charge carriers migration behaviours in photocatalysts according to the fluorogenic redox reaction detected by a single-molecule fluorescence microscopy is difficult to directly relate to their activities on the targeted functions such as proton reduction [14]. Even though the performances of ensemble photocatalysts could be achieved easily, the information on single-particle level is still rare. On the contrary, the photoluminescence (PL) signals, such as intensity and lifetime, measured on a single semiconductor particle are able to reflect its photocatalytic activities according to the established correlation. Thereby, single-particle PL study is a more direct strategy to illustrate the photocatalytic activity of single particle compared with ensemble methods. Additionally, for further activity enhancement, surface modifications, especially loading co-catalyst to form heterostructure, are always employed [15]. Although the fundamental mechanisms of heterostructure photocatalysts have already been established, direct *in situ* monitoring the PL intensity variations in a real time focusing on individual particle during the formation of heterostructure has been rarely studied [16].

Recently, using low-cost metal sulfides such as MoS_2, CuS, and NiS

* Corresponding author.
E-mail address: majima@sanken.osaka-u.ac.jp (T. Majima).

https://doi.org/10.1016/j.apcatb.2019.05.031
Received 18 March 2019; Received in revised form 3 May 2019; Accepted 7 May 2019
Available online 08 May 2019
0926-3373/

instead of noble metals as co-catalyst for hydrogen evolution is a working target [17–19]. It has been reported that NiS nanoparticles (NiS) are formed on semiconductors under light irradiation in water solution at room temperature, making it applicable for *in situ* studies, since the traditional methods for synthesizing NiS, such as hydrothermal or sulfidization, need harsh conditions, high temperature or pressure [20–23]. In the present work, a single-particle PL microscopy was used to *in situ* observe the PL intensity change during NiS photodeposition on individual TMC particle, which was closely related to their photocatalytic performance. The straightforward visualization using single-particle PL technique provided strong evidences on the preferred deposition of NiS at the lateral plane of TMC and efficient electron migration from TMC to NiS in TMC/NiS heterostructure, resulting in a greatly enhanced photocatalytic activity for H_2 evolution.

2. Experimental

2.1. Synthesis of TiO_2 mesocrystal (TMC)

TMC was prepared following our previous study [24]. A precursor aqueous solution of TiF_4 (Wako Pure Chemical Industries), ultrapure H_2O, NH_4NO_3 (Sigma-Aldrich), and NH_4F (Wako Pure Chemical Industries) with the molar ratio of 1:117:6.6:4 was dropped on a silicon wafer dropwise to form a thin layer. The thickness of the aqueous solution layer should be no more than 1 mm. The precursor was annealed in air at 500 °C for 2 h with a ramping rate of 10 °C min^{-1}. The obtained product was collected and then annealed at 500 °C in oxygen atmosphere for another 8 h to remove surface impurities.

2.2. Synthesis of TMC/NiS

Photodeposition of NiS on TMC surface is based on reported work with some modifications [20]. Instead of $Ni(CH_3COO)_2$, $NiCl_2{\cdot}6H_2O$ was chosen as the precursor of NiS. In detail, 20 mg TMC powder was added into a mixture solution of *X* mL $NiCl_2{\cdot}6H_2O$ (Wako Pure Chemical Industries) aqueous solution (11.9 mg mL^{-1}), *X* mL thiourea (Wako Pure Chemical Industries) aqueous solution (38 mg mL^{-1}), 4 mL ethanol and (6 - 2*X*) mL ultrapure H_2O. Subsequently, the suspension was dearated Argon gas for 30 min to remove air and then irradiated under 365-nm LED for 30 min at room temperature. Finally, the product was centrifuged and washed by water and ethanol three times, and freeze dried. By varying the amount of $NiCl_2$ and thiourea (*X*) added in the suspension, different deposition content of NiS could be achieve, named as TMC/NiS-*X*. The detailed amount of loading NiS was measured by inductively coupled plasma mass spectrometry (ICP-MS).

2.3. Characterizations

The samples were characterized using X-ray diffraction (XRD, Rigaku Rint-2500, CuKα source), scanning electron microscopy (SEM, JEOL JSM-6330FT), transmission electron microscopy (TEM, JEOL, 2100, operated at 100 KV), and high-resolution TEM (JEM-3000F, operated at 300 KV). UV–vis absorption spectra were obtained on a JASO V-570 UV–vis/NIR spectrophotometer. X-ray photoelectron spectroscopy (XPS) was performed with a JEOL JPS-9010 MC spectrometer. The adventitious carbon (C 1s located at 284.6 eV) was used as reference to binding energy. The concentration of NiS was determined byinductively coupled plasma mass spectrometry (Shimadzu, ICPS-8100).

2.4. In situ monitoring photodeposition process of NiS on TMC using confocal single-particle PL microscopy

The quartz cover glasses are purchased from DAICO MFG CO., Ltd. (Japan) and cleaned by sonication in a 40% detergent solution (As One, Cleanace) for 7 h, followed by repeated washings with warm water for 6 times. Finally, the cover glasses were washed again using ultrapure water before using. Well dispersed TMC ethanol solution was spin-coated on the cleaned cover glasses. Subsequently, the cover glasses were annealed under 60 °C for 1 h to immobilize the particles. A small chamber was attached on the cover glass which served as reaction vessel. We prepared the reaction solution containing 1.5 mL $NiCl_2$ aqueous solution (11.9 mg mL^{-1}), 1.5 mL thiourea aqueous solution (38 mg mL^{-1}), 4 mL ethanol, and 3 mL ultrapure water. 20 μL such solution was added into the chamber. A box with UV lamp fixed on the top was placed on the cover glass and then dearated Argon gas for 30 min to make sure that the amount of oxygen is less than 1%. Then the UV lamp was turned on to irradiate the chamber perpendicular for certain times.

The single-particle PL signals from individual sample was recorded using an objective-scanning confocal microscope system (PicoQuant, MicroTime 200) coupled with an Olympus IX71 inverted fluorescence microscope. The samples spin-coated on clean cover glass were excited through an oil objective (Olympus, UplanSApochromat, 1.40 numerical aperture, ×100) with a circular-polarized 385-nm pulsed laser (Spectra-Physics, MAI TAI HTS-W provided with an automated frequency double, Inspire Blue FAST-W; 0.8 MHz repetition rate, 10 μW excitation power) controlled by a PDL-800B driver (PicoQuant). For the spectroscopy, only the emission that passed through a slit entered the imaging spectrograph (Acton Research, SP-2356) that was equipped with an electron-multiplying charge-coupled device (EMCCD) camera (Princeton Instruments, ProEM). All of the experimental data were achieved at room temperature.

2.5. Single-particle PL measurements

Single-particle PL image and PL spectra were obtained as described in the above section. For decay profile, the emission was collected with the same objective and detected by a single photon avalanche photodiode (Micro Photon Devices, PDM 50CT) through a dichroic beam splitter (Chroma, z405/488rpc), a long-pass filter (Chroma, HQ510LP), and a 50 μm pinhole for spatial filtering to reject out-of-focus signals. The data collected using the PicoHarp 300 TCSPC module (PicoQuant) were stored in the time-tagged time-resolved mode, recording every detected photon with its individual timing.

2.6. Photocatalytic hydrogen evolution

3 mg sample were dispersed in 5 mL aqueous solution containing 20 vol% methanol using an ultrasonic bath. Subsequently, the suspension was bubbled with argon gas through the reactor for 30 min to completely remove the dissolved oxygen and ensure that the reactor was in an anaerobic condition. The samples were irradiated under 365-nm UV LED for H_2 evolution at room temperature. The volume of H_2 was measured by Shimadzu GC-8A gas chromatograph equipped with an MS-5A column and thermal conductivity detector. The catalytic stability was evaluated by isolating, washing and reusing the catalyst in a cycling experiment. The apparent quantum efficiency (AQE) was carried out under different wavelength irradiation using a Xenon lamp and calculated using the following equation [25],

$$\mathrm{AQE}\ (\%) = \frac{\text{Number of evolved } H_2 \text{ molecules} \times 2}{\text{Number of incident photons}} \times 100\%.$$

2.7. Photoelectrochemical measurements

Electrochemical and photoelectrochemical measurements were performed in three-electrode quartz cells. Platinum wire was used as the counter electrode, and Ag/AgCl electrode were used as the reference electrodes, respectively. For loading sample film electrodes on glassy carbon, 4 mg sample was added into solution containing H_2O and CH_3CH_2OH with volume ratio of 1:1. Then 50 μL Nafion was added into

the solution. After ultrasonic for 10 min, 3 μL solution was dropped on the surface of glassy carbon with the diameter of 1.5 mm (surface area 0.071 cm^2). The electrode was used for photoelectrochemical measurements after drying. 0.5 M Na_2SO_4 aqueous solution was used as the electrolyte. Electrochemical impedance spectroscopy (EIS) was carried out under simulated solar light irradiation. The Xenon lamp was utilized as the light source in the photoelectrochemical measurements.

3. Results and discussion

TMC was synthesized through a one-step, template-free, and topotactic transformation annealing process [9,10]. Scanning electron microscopy (SEM) and transmission electron microscopy (TEM) images of TMC (Fig. S1) showed a plate-like porous structure with several to tens micrometers assembled by single crystalline TiO_2 nanoparticles as building blocks regularly. To fabricate TMC/NiS-*X* heterostructure, *X* mL of $NiCl_2$ and *X* mL of thiourea were added into as-prepared 20 mg TMC aqueous dispersions with magnetic stirring. The solution was dearated for 30 min and then photoirradiated under 365-nm light source for another 30 min. After photodeposition process, NiS with about 10-nm diameter were formed on the surface of TMC, especially at the lateral planes (Fig. 1a). While the TMC still kept its morphology and structure after light irradiation (Fig. S2). The clear lattice fringes of 0.335, 0.189, and 0.196 nm shown in high resolution TEM (HRTEM, Fig. 1b) corresponded to (101) and (200) facets of TiO_2 and (102) facet of NiS, respectively [20,26,27]. Importantly, NiS were closely contacted with {101} facet of TMC.

Elemental mapping analysis also confirmed the formation of NiS through photoreduction process (Fig. 1c–f). Even though there were NiS on the basal plane of TMC, more nanoparticles were deposited on the lateral plane, which was in accordance with the TEM results. Therefore, it is obvious that more photogenerated electrons in TMC migrated to the lateral plane of TMC, where the photoreduction reaction took place to form NiS (Fig. 1g). An energy dispersive X-ray spectroscopy (EDX) of selected area further confirmed the existence of NiS on TMC (Fig. S3). The contents of Ni and Ti atoms were examined by inductively coupled plasma mass spectrometry (ICP-MS) as shown in Table S1. Interestingly, the weight percent of NiS was relatively low (less than 1.0 wt%) even a large amount of NiS precursor was added, indicating that only a part of $NiCl_2$ and thiourea turned to NiS.

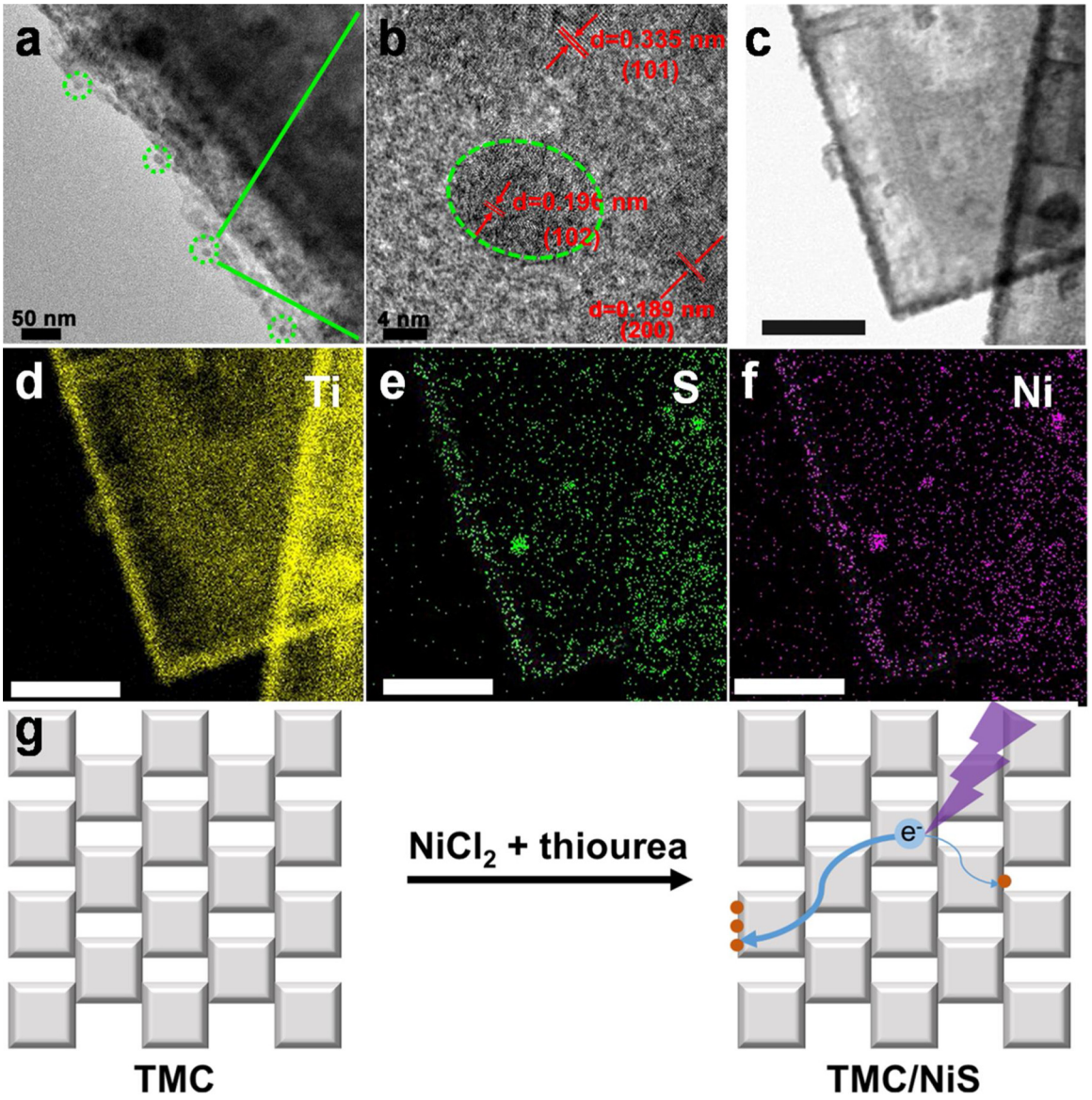

Fig. 1. TEM (a) and HRTEM (b) images of TMC/NiS-1.5 (the amount of NiS is 0.65 wt%). TEM image (c) and elemental mapping of Ti (d), S (e), and Ni (f) of TMC/NiS-1.5. The scale bar is 0.5 μm. (g) Scheme for the photodeposition of NiS on TMC superstructure under 365-nm photoirradiation.

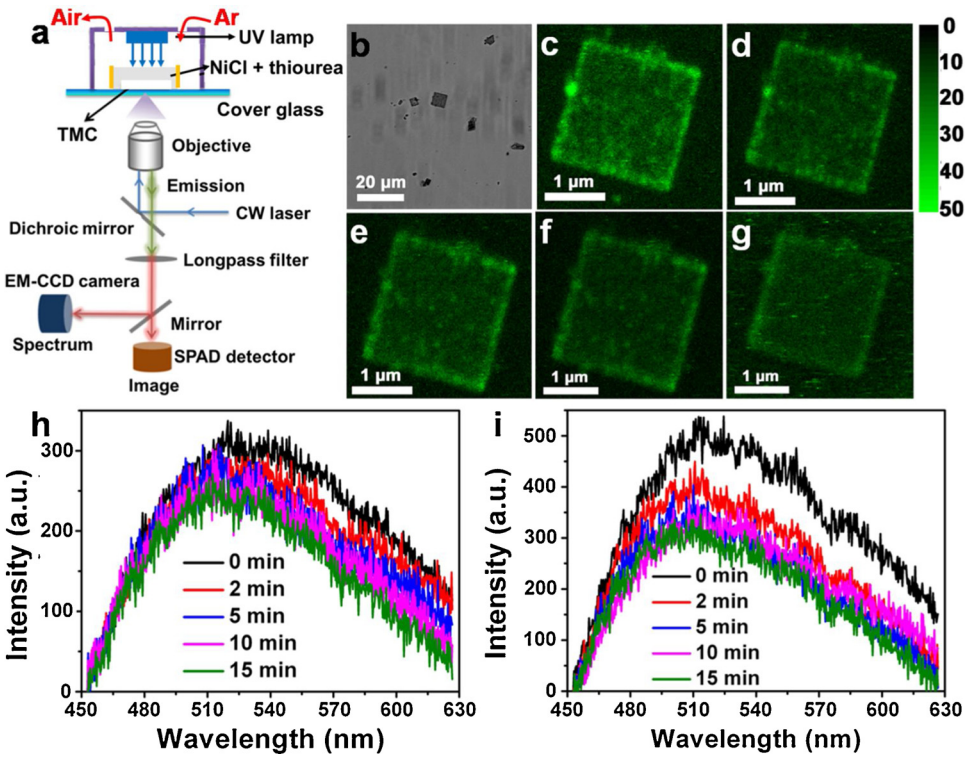

Fig. 2. Schematic illustration of a confocal microscopy measurement for monitoring *in situ* NiS photodeposition on a single TMC particle (a). Optical transmission image of TMC immobilized on a quartz glass in $NiCl_2$ and thiourea aqueous solution (b). PL emission images of TMC particle after photoirradiation at 385-nm for 0 min (c), 2 min (d), 5 min (e), 10 min (f), and 15 min (g). Representative PL spectra of TMC at the center (h) and edge (i).

X-ray diffraction (XRD) patterns of TMC and TMC/NiS-X powders revealed a pure anatase structure of TiO_2 for all samples (Fig. S4). No diffraction peaks of NiS could be observed probably due to the weak crystallization and low loading amount [28,29]. The chemical components of each element in TMC/NiS-1.5 were investigated by X-ray photoelectron spectroscopy (XPS) spectra (Fig. S5). For the Ti 2p and O 1s spectra, characteristic peaks located at 459.0, 464.7, 530.3, and 532.2 eV were assigned to Ti $2p_{3/2}$, Ti $2p_{1/2}$, Ti-O in TiO_2 and chemisorbed water, respectively [30–32]. The binding energies of two main peaks at 856.3 and 861.7 eV corresponded to Ni $2p_{3/2}$ and Ni $2p_{1/2}$, respectively. The S 2p peaks at 162.4 and 163.7 eV were also in accordance with the sulfur element in NiS [20,33,34]. Therefore, the TEM images and XPS analysis clearly confirmed the successful formation of NiS on TMC.

As mentioned before, single-particle PL imaging technique is a powerful tool for investigating transport behaviors of photogenerated charge carriers on individual particle scale and thus forecasting the photocatalytic activity of semiconductors. In order to obtain a direct visual information, PL changes were *in situ* monitored during the NiS photodeposition on a single TMC particle in aqueous solution. Fig. 2a shows a confocal PL microscopy used for the single-particle detection in the present study. TMC particles were firstly coated on a quartz cover glass with single-particle dispersion and heated at 60 °C for 1 h for immobilization. A micro-chamber was attached on the quartz cover glass as a reaction vessel (Fig. S6). A 365-nm UV lamp was fixed at the top of box to ensure that it could irradiate the chamber perpendicular. Before measurement, the reaction chamber was deaerated Ar gas for 30 min to remove oxygen (less than 1%). The detailed processes are given in supporting information.

One typical TMC particle was chosen from low magnification bright-field micrographs as shown in the selected area in optical transmission image (Fig. 2b). Correspondingly, the emission image was achieved under 385-nm laser excitation before UV lamp irradiation (named as 0 min). A broad emission spectrum appeared in 450–630 nm region as shown in Fig. 2h and i, resulting from the recombination of electron-hole pairs at TMC surface [35,36]. Interestingly, the PL intensity increased from the basal plane (300 counts) to the lateral plane (500 counts). Then we stopped the PL imaging and irradiated the TMC particle for a certain time (2, 5, 10, and 15 min) using the 365-nm UV lamp. At each irradiation time, we recorded the PL emission images and spectra as shown in Fig. 2c–i. It is clear that the PL intensity of TMC decreased gradually as the irradiation time prolonged, suggesting the surface conditions change on TMC. After the first 5 min, the PL intensity of TMC was quenched greatly due to the fast loading of NiS. While after 15 min, the PL intensity showed very little decrease in contrast with the product after irradiation for 10 min, indicating the almost complete of photodeposition process. More importantly, the PL intensity at the lateral plane of TMC exhibited a more significant decrease compared with that at the basal plane, as supported by the PL spectra (Fig. 2h and i). Additionally, the PL images of individual TMC particle were also recorded without adding $NiCl_2$ solution, and there was no obvious variation after irradiating under 365-nm UV lamp for 20 min, suggesting that the deposited NiS led to the PL intensity quenching of TMC (Fig. S7). Generally, a higher PL intensity means a faster recombination rate of photoexcited electron-hole pairs in semiconductors [10,37]. Such PL quenching clearly indicated the existence of electron transfer from TMC to NiS which suppressed the radiative charge recombination in TMC.

In order to further study and gain more precise information of charge transfer properties in TMC/NiS heterostructure, single-particle PL measurement was performed on pure TMC and as-synthesized TMC/NiS-1.5 sample. PL signals of both TMC and TMC/NiS-1.5 were measured under a 385-nm pulsed laser irradiation in ambient air condition. It has been found that the PL intensity of particles is greatly related to their surrounding environments, and the PL intensity measured in air is greatly higher than that in aqueous solution [38]. Compared with TMC, the heterostructure displayed an obvious PL quenching under the same condition (Fig. 3c and d). The emission intensity at lateral plane of TMC/NiS-1.5 was quenched about 75%, which was more than that at basal plane (67%) (Fig. 3e). In addition, we also randomly chose other TMC and TMC/NiS-1.5 particles and measured their PL emission images and spectra under air conditions as shown in Figs. S8 and S9. After photodeposition of NiS, the PL emission intensities at both basal and lateral planes of TMC were greatly decreased, and the PL intensity at

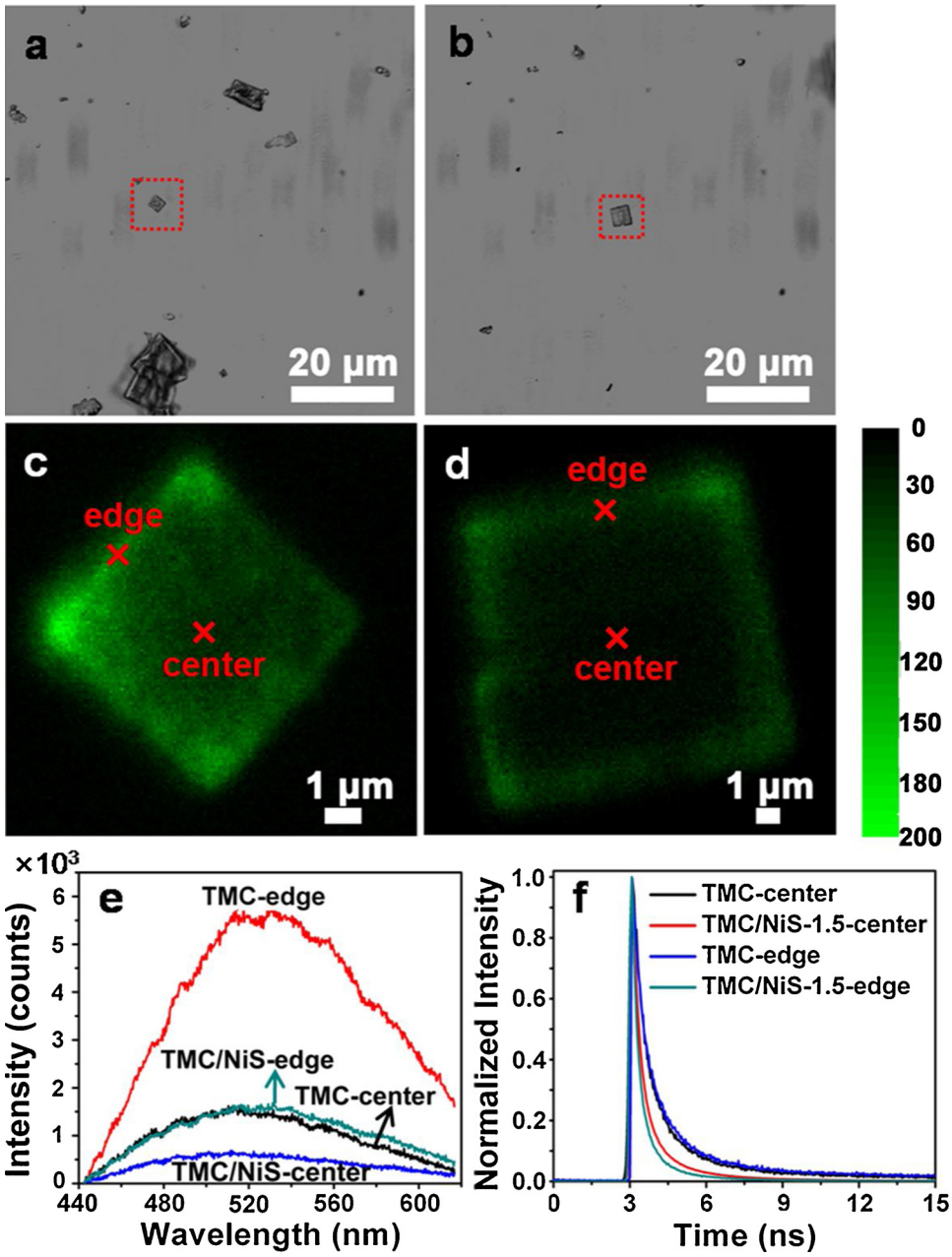

Fig. 3. Optical transmission images of pure TMC (a) and TMC/NiS-1.5 (b). PL emission images of pure TMC (c) and TMC/NiS-1.5 (d). Emission spectra (e) and emission decay profiles (f) observed at basal and lateral planes on both pure TMC and TMC/NiS-1.5.

lateral planes exhibited more obvious quenching than that at basal planes.

Even though the existence of interfacial electron transfer has been demonstrated by PL intensity change, the kinetic characteristics were still unclear and time-resolved PL decays were, therefore, carefully investigated as shown in Fig. 3f. The corresponding fitting parameters were summarized in Table 1. Consistent with emission intensity, the average PL lifetime (τ_{ave}) in single TMC exhibited small variations in different positions as the τ_{ave} value at the basal plane was 3.0 ns and then increased to 3.7 ns at lateral surface. Such phenomenon is due to the different recombination probability between center and edge [10]. In the case of TMC/NiS-1.5, the τ_{ave} was greatly shortened from 3.7 to 1.0 ns at lateral plane and from 3.0 to 1.5 ns at basal plane, respectively. According to the equation: $k_{ET} = <\tau_{ave}(TMC/NiS\text{-}1.5)>^{-1} - <\tau_{ave}(TMC)>^{-1}$, the rate constant for electron transfer process at lateral plane was calculated to be 7.3×10^{10} s^{-1}, which was 2.2 times

Table 1
Lifetimes from exponential curve fitted analysis of time-resolved PL decays for TMC and TMC/NiS-1.5.

Sample	τ_1 (ns)	τ_2 (ns)	τ_{ave} (ns)[a]
TMC-center	0.71 ± 0.04 (82%)	4.6 ± 0.32 (19%)	3.0
TMC-edge	0.79 ± 0.06 (84%)	5.8 ± 0.43 (16%)	3.7
TMC/NiS-1.5-center	0.51 ± 0.03 (87%)	2.8 ± 0.19 (13%)	1.5
TMC/NiS-1.5-edge	0.35 ± 0.03 (91%)	2.2 ± 0.12 (8.6%)	1.0

[a] The multi-exponential decay curves were fitted using a nonlinear least-squares method with a multi-component decay law given by $\Delta A = \Delta A_0 + \sum_i A_i e^{\left(-\frac{t}{\tau_i}\right)}$, where A and τ refer the amplitudes and lifetimes, respectively. The average lifetime τ_{ave} was then determined using the equation:

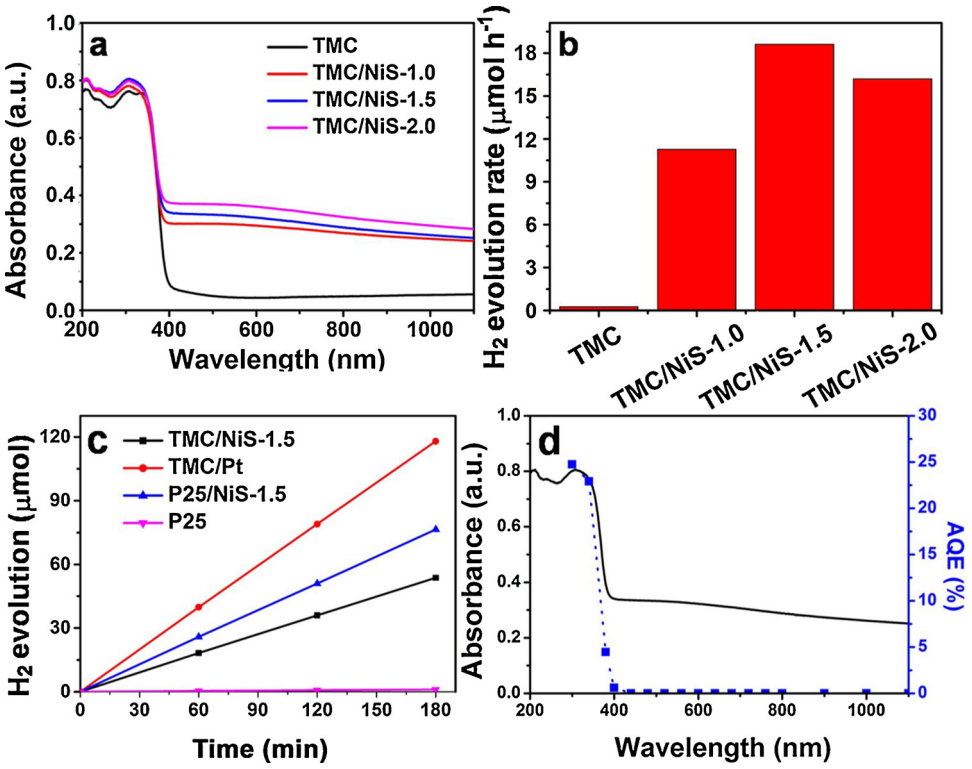

Fig. 4. (a) UV–vis absorption spectra of TMC and TMC/NiS-*X*. (b) Comparison of photocatalytic H_2 evolution activities of different samples. (c) Photocatalytic H_2 evolution from water on different catalysts under 365-nm photoirradiation. (d) Wavelength dependence of the apparent quantum efficiency for TMC/NiS-1.5.

faster than that at the basal plane (3.3×10^{10} s^{-1}) [39,40]. As a more important value for evaluating photocatalytic activity, the electron transfer efficiency (η_{ET}) from TMC to NiS was also estimated based on the equation: $\eta_{ET} = 1 - (\tau_{ave}(TMC/NiS\text{-}1.5)/\tau_{ave}(TMC))$ [40]. Similar to the rate constant, the lateral plane of TMC exhibted a much higher efficiency (73%) than the basal plane (50%). We also recorded the PL decay curves of TMC/Pt at both lateral and basal palnes and fitted exponentially (Fig. S10). Similar to TMC/NiS-1.5, the average lifetimes of TMC/Pt at both sites decreased considerably, and the lifetime at the lateral plane (0.80 ns) was much shorter than that at the basal plane (1.22 ns), which is consistent with the previous result [10]. Moreover, we calculated the electron injection efficiency in TMC/Pt according to the equation of $\eta_{ET} = 1 - (\tau_{ave}(TMC/NiS\text{-}1.5)/\tau_{ave}(TMC))$. It is demonstrated that the lateral plane (84%) exhibits higher electron injection efficiency than the basal plane (59%), which is similar to TMC/NiS-1.5. Considering the TEM and elemental mapping images, we could conclude that the preferrable photodeposition of NiS at the lateral plane of TMC lead to a more efficient interfacial charge injection from TMC to NiS.

Photoelectrochemical measurements were also used to demonstrate the interfacial electron transport in TMC/NiS heterostructures. Transient photocurrent (*I-t*) curves recorded for several on-off cycles of intermittent light irradiation are illustrated in Fig. S11. All electrodes displayed rapid and repeatable on/off cycles of photocurrent densities when they were served as working electrodes under simulated solar light irradiation. TMC/NiS-*X* samples showed an obvious enhancement compared with pure TMC, and TMC/NiS-1.5 exhibited the highest average photocurrent density with11 μA cm^{-2} to be 5.5 folds enhanced than that of TMC (2.0 μA cm^{-2}). In addition, electrochemical impedance spectra (EIS) of all above electrodes were measured to investigate the electrical conductivity (Fig. S12). Generally, a larger diameter of semicircle arc (DSA) represents a higher transfer resistance [41–44]. TMC/NiS-1.5 possessed the smallest DSA among all samples, indicating that the photogenerated electrons in TMC/NiS-1.5 had fastest mobility. These photoelectrochemical results together with PL changes confirmed the retardation of electron-hole pairs recombination in TMC/NiS heterostructure, which would lead to an enhanced photocatalytic activity.

Prior to the photocatalytic performance measurements, the optical properties of all samples were firstly measured by UV–vis absorption spectra (Fig. 4a). The absorption edge of TMC was approximately 400 nm, corresponding to the intrinsic absorption of TiO_2 (~ 3.1 eV). Photodeposition of NiS greatly influenced the optical properties of samples. With increasing the amount of NiS, light absorption in the range from 400 to 1100 nm was gradually enhanced, while the bandgap of TMC/NiS-*X* did not change. The corresponding photo images of samples were shown in Fig. S13.

The H_2 evolution rates of all photocatalysts were measured under 365-nm photoirradiation in the presence of 20 vol% methanol as sacrificial reagent (Fig. 4b). When pure TMC was served as the photocatalyst, only 0.26 μmol H_2 was detected within one hour. While for the TMC/NiS-*X* heterostructures, the photocatalytic performances were dramatically enhanced, and TMC/NiS-1.5 sample exhibited the highest H_2 evolution rate with 18.6 μmol h^{-1} to be approximately 71 folds higher than that of TMC. Due to the low content of NiS in heterostructures according to ICP-MS measurements and the well-kept morphology and porous structure of TMC after photodeposition process, the surface area of TMC/NiS-*X* samples would not increase compared with pure TMC. Therefore, the deposited NiS greatly retarded the recombination of electron-hole pairs in TMC, leading to an enhanced photocatalytic activity. Additionally, the H_2 evolution rate of P25 is also greatly enhanced after photodeposition of NiS to be about 25.5 μmol h^{-1} (Fig. 4c). Such dramatic enhancement proved that NiS not only enhanced the charge carriers separation efficiency, but also acted as the active site for water splitting reaction (Scheme S1) [19,34]. It has been reported that the deposition of single co-catalyst would change the direction of built-in electric fields beneath the uncovered surface of TMC, in which photogenerated electrons migrate to NiS over distances that are much longer than their diffusion length [45]. Therefore, the surface density of accumulated electrons is enhanced to be beneficial

for photocatalysis.

As a commonly used co-catalyst, Pt exhibits excellent activity for H_2 evolution. The high cost and scarcity of Pt, however, limits its further application. Here, the photocatalytic activity of TMC after hybriding 3 wt% Pt was also measured to check whether NiS can be replaced for Pt as an efficient co-catalyst. It demonstrated that the H_2 evolution rate of TMC/NiS-1.5 was almost 50% of the activity when Pt was harnessed as co-catalyst (39.3 μmol h^{-1}, Fig. 4c). While considering the price and abundance, NiS would be a more promising co-catalyst for photocatalytic H_2 evolution. Wavelength dependence of the apparent quantum efficiency (AQE) was also estimated using various band-pass filters under the same reaction conditions as shown in Fig. 4d. The trend of AQE closely followed those of absorbance measured by UV-DRS to reach up to 25.0% and 22.5% at 340 and 360 nm, respectively. The stability of TMC/NiS-1.5 was further tested and there was no obvious decrease after 3 cycles (Fig. S14). Elemental mapping of TMC/NiS-1.5 after the test also indicated that NiS were still anchored on the surface of TMC, suggesting a good stability and tight connection between NiS and TMC (Fig. S15).

4. Conclusions

In summary, TMC/NiS heterogeneous photocatalysts were synthesized by a simple photodeposition method. The process of NiS loading on single TMC particle was *in situ* monitored based on the PL intensity change by a single-particle PL microscopy. The PL intensity and averaged lifetime of TMC gradually decreased during the formation of NiS, and the lateral planes of TMC exhibited a more obvious PL quenching and lifetime shortening compared with the basal planes, confirming the preferred deposition of NiS on the lateral surface and more efficient electron injection from the lateral planes of TMC to NiS. As a result, the photocatalytic H_2 evolution for TMC/NiS-*X* under 365-nm photoirradiation was significantly enhanced and TMC/NiS-1.5 sample exhibited the highest activity with 18.6 μmol h^{-1} to be 71 times higher than that of pure TMC particles. The present work provides a straightforward visual evidence for deep understanding the chemical reaction on single particle scale and establishing structure-reactivity relationships.

Conflicts of interest

There are no conflicts of interest to declare.

Acknowledgements

We thank to Drs. Mingshan Zhu and Zaizhu Lou, SANKEN, Osaka University for their discussion. This work has been partly supported by a Grant-in-Aid for Scientific Research (Project 25220806 and others) from the Ministry of Education, Culture, Sports, Science and Technology (MEXT) of the Japanese Government. We are thankful for the help of the Comprehensive Analysis Center of SANKEN, Osaka University.

Appendix A. Supplementary data

Supplementary material related to this article can be found, in the online version, at doi:https://doi.org/10.1016/j.apcatb.2019.05.031.

References

[1] I.L.C. Buurmans, B.M. Weckhuysen, Nat. Chem. 4 (2012) 873.
[2] T. Chen, B. Dong, K. Chen, F. Zhao, X. Cheng, C. Ma, S. Lee, P. Zhang, S.H. Kang, J.W. Ha, W. Xu, N. Fang, Chem. Rev. 117 (2017) 7510–7537.
[3] R.M. Crooks, M. Zhao, L. Sun, V. Chechik, L.K. Yeung, Acc. Chem. Res. 34 (2001) 181–190.
[4] B.M. Weckhuysen, ChemInform 36 (2005).
[5] T. Tachikawa, T. Majima, Chem. Soc. Rev. 39 (2010) 4802–4819.
[6] P. Chen, X. Zhou, N.M. Andoy, K.-S. Han, E. Choudhary, N. Zou, G. Chen, H. Shen, Chem. Soc. Rev. 43 (2014) 1107–1117.
[7] K.P.F. Janssen, G. De Cremer, R.K. Neely, A.V. Kubarev, J. Van Loon, J.A. Martens, D.E. De Vos, M.B.J. Roeffaers, J. Hofkens, Chem. Soc. Rev. 43 (2014) 990–1006.
[8] R. Chen, F. Fan, T. Dittrich, C. Li, Chem. Soc. Rev. 47 (2018) 8238–8262, https://doi.org/10.1039/C8CS00320C.
[9] Z. Bian, T. Tachikawa, T. Majima, J. Phys. Chem. Lett. 3 (2012) 1422–1427.
[10] Z. Bian, T. Tachikawa, W. Kim, W. Choi, T. Majima, J. Phys. Chem. C 116 (2012) 25444–25453.
[11] Z. Bian, T. Tachikawa, P. Zhang, M. Fujitsuka, T. Majima, J. Am. Chem. Soc. 136 (2014) 458–465.
[12] M. D'Arienzo, J. Carbajo, A. Bahamonde, M. Crippa, S. Polizzi, R. Scotti, L. Wahba, F. Morazzoni, J. Am. Chem. Soc. 133 (2011) 17652–17661.
[13] J. Yu, J. Low, W. Xiao, P. Zhou, M. Jaroniec, J. Am. Chem. Soc. 136 (2014) 8839–8842.
[14] M. Hesari, X. Mao, P. Chen, J. Am. Chem. Soc. 140 (2018) 6729–6740.
[15] J. Ran, J. Zhang, J. Yu, M. Jaroniec, S.Z. Qiao, Chem. Soc. Rev. 43 (2014) 7787–7812.
[16] A. Demortière, R.D. Schaller, T. Li, S. Chattopadhyay, G. Krylova, T. Shibata, P.C. dos Santos Claro, C.E. Rowland, J.T. Miller, R. Cook, B. Lee, E.V. Shevchenko, J. Am. Chem. Soc. 136 (2014) 2342–2350.
[17] B. Hinnemann, P.G. Moses, J. Bonde, K.P. Jørgensen, J.H. Nielsen, S. Horch, I. Chorkendorff, J.K. Nørskov, J. Am. Chem. Soc. 127 (2005) 5308–5309.
[18] J. Zhang, J. Yu, Y. Zhang, Q. Li, J.R. Gong, Nano Lett. 11 (2011) 4774–4779.
[19] C. Xue, H. Li, H. An, B. Yang, J. Wei, G. Yang, ACS Catal. 8 (2018) 1532–1545.
[20] H. Zhao, H. Zhang, G. Cui, Y. Dong, G. Wang, P. Jiang, X. Wu, N. Zhao, Appl. Catal. B: Environ. 225 (2018) 284–290.
[21] W. Zhang, Y. Wang, Z. Wang, Z. Zhong, R. Xu, Chem. Commun. 46 (2010) 7631–7633.
[22] J. Yuan, J. Wen, Y. Zhong, X. Li, Y. Fang, S. Zhang, W. Liu, J. Mater. Chem. A 3 (2015) 18244–18255.
[23] L.S. Zhang, Y.P. Huang, Y.F. Zhang, H.H. Gu, W. Fan, T.X. Liu, Adv. Energy Mater. 3 (2016) 1500467.
[24] O. Elbanna, M. Fujitsuka, T. Majima, ACS Appl. Mater. Interfaces 9 (2017) 34844–34854.
[25] K. Chang, X. Hai, J. Ye, Adv. Energy Mater. 6 (2016) 1502555.
[26] M. Xie, X. Fu, L. Jing, P. Luan, Y. Feng, H. Fu, Adv. Energy Mater. 4 (2014) 1300995.
[27] W. Li, J. Yang, Z. Wu, J. Wang, B. Li, S. Feng, Y. Deng, F. Zhang, D. Zhao, J. Am. Chem. Soc. 134 (2012) 11864–11867.
[28] P. Zhang, T. Wang, X. Chang, L. Zhang, J. Gong, Angew. Chem. Int. Ed. 55 (2016) 5851–5855.
[29] Q. Zhai, S. Xie, W. Fan, Q. Zhang, Y. Wang, W. Deng, Y. Wang, Angew. Chem. Int. Ed. 125 (2013) 5888–5891.
[30] X. Shi, M. Fujitsuka, Z. Lou, P. Zhang, T. Majima, J. Mater. Chem. A 5 (2017) 9671–9681.
[31] J.C. Yu, W. Ho, J. Yu, S.K. Hark, K. Iu, Langmuir 19 (2003) 3889–3896.
[32] B. Chai, T. Peng, J. Mao, K. Li, L. Zan, Phys. Chem. Chem. Phys. 14 (2012) 16745–16752.
[33] Z. Chen, P. Sun, B. Fan, Z. Zhang, X. Fang, J. Phys. Chem. C 118 (2014) 7801–7807.
[34] P. Luo, H. Zhang, L. Liu, Y. Zhang, J. Deng, C. Xu, N. Hu, Y. Wang, ACS Appl. Mater. Interfaces 9 (2017) 2500–2508.
[35] T. Tachikawa, S. Yamashita, T. Majima, J. Am. Chem. Soc. 133 (2011) 7197–7204.
[36] T. Tachikawa, T. Ishigaki, J.-G. Li, M. Fujitsuka, T. Majima, Angew. Chem. Int. Ed. 47 (2008) 5348–5352.
[37] Y.J. Li, Y.J. Xue, J. Tian, X.J. Song, X.J. Zhang, X.Z. Wang, H.Z. Cui, Sol. Energy Mater. Sol. Cells. 168 (2017) 100–111.
[38] Z. Lou, S. Kim, P. Zhang, X. Shi, M. Fujitsuka, T. Majima, ACS Nano 11 (2017) 968–974.
[39] I. Robel, M. Kuno, P.V. Kamat, J. Am. Chem. Soc. 129 (2007) 4136–4137.
[40] W.-J. Ong, L.K. Putri, Y.-C. Tan, L.-L. Tan, N. Li, Y.H. Ng, X. Wen, S.-P. Chai, Nano Res. 10 (2017) 1673–1696.
[41] M. Adachi, M. Sakamoto, J. Jiu, Y. Ogata, S. Isoda, J. Phys. Chem. B 110 (2006) 13872–13880.
[42] X. Shi, M. Fujitsuka, S. Kim, T. Majima, Small 14 (2018) 1703277.
[43] D.H. Xia, H.D. Liu, B.H. Xu, Y.C. Wang, Y.H. Liao, Y.J. Huang, L.Q. Ye, C. He, P.K. Wong, R.L. Qiu, Appl. Catal. B: Environ. 245 (2019) 177–189.
[44] L.L. Hu, H.J.W. He, D.H. Xia, Y.J. Huang, J.R. Xu, H.Y. Li, C. He, W.J. Yang, D. Shu, P.K. Wong, ACS Appl. Mater. Interfaces 10 (2018) 18693–18708.
[45] J. Zhu, S. Pang, T. Dittrich, Y. Gao, W. Nie, J. Cui, R. Chen, H. An, F. Fan, C. Li, Nano Lett. 17 (2017) 6735–6741.